Single-cell metabolic analysis by mass cytometry reveals distinct transitional states of CD8 T cell differentiation

Lauren S. Levine[1-6*], Kamir J. Hiam[2-6*], Diana M. Marquez[2-6], Iliana Tenvooren[2-6], Diana C. Contreras[7], Jeffrey C. Rathmell[7], Matthew H. Spitzer[2-6]

1. Department of Medicine, University of California San Francisco, San Francisco, CA 94143
2. Helen Diller Family Comprehensive Cancer Center, University of California San Francisco, San Francisco, CA 94158
3. G.W. Hooper Research Foundation, Department of Immunology and Microbiology, University of California San Francisco, San Francisco, CA 94143
4. Department of Otolaryngology, University of California San Francisco, San Francisco, CA 94143
5. Chan Zuckerberg Biohub, San Francisco, CA 94158
6. Parker Institute for Cancer Immunotherapy, San Francisco, CA 94129
7. Vanderbilt Center for Immunobiology, Department of Pathology, Microbiology, and Immunology, Vanderbilt University Medical Center, Nashville, TN 37232

Correspondence: matthew.spitzer@ucsf.edu

*These authors contributed equally to this work.

Abstract

Mass cytometry permits high-dimensional analysis of diverse aspects of cellular behavior. Here, we adapted this platform to simultaneously profile metabolism, signaling, cell cycle, and effector function with single-cell resolution. Using this approach, we measured enzymes characterizing glycolysis, the TCA cycle, fatty acid oxidation, oxidative phosphorylation, and nutrient transport. In conjunction, we measured downstream targets of TCR signaling regulating translation, proliferation and cytotoxicity as well as surface markers and transcription factors delineating CD8 T cell differentiation. High-dimensional single-cell metabolic analysis by mass cytometry permits identification of unique metabolic and differentiation states of extremely rare cell populations, such as antigen-specific T cells. We interrogated antigen-specific CD8 T cell activation *in vitro* as well as the trajectory of CD8 T cells responding to *Listeria monocytogenes* infection, a well-characterized model for studies of T cell differentiation. This integrated, high-dimensional approach revealed a novel, activated, and highly metabolically active transitional T cell subset emerging at four days post-infection. These cells simultaneously exhibit glycolytic and oxidative functional programs, which we propose represents a key metabolic inflection point in CD8+ T cell differentiation. This approach should be useful for mechanistic investigations of metabolic regulation of immune responses *in vivo.*

Introduction

As the appreciation of the importance of immune responses to the propagation and maintenance of healthy and diseased states increases, understanding the regulatory mechanisms underlying immune cell function and fate has become crucial to developing more rationally designed treatment strategies for acute and chronic infections, autoimmune diseases and malignancy[1]. CD8 T cells have been a central focus of these efforts due to their ability generate long-term memory responses, which confer durable protection against re-infection and cancer relapse[2,3]. The field of immunometabolism has provided critical insight into these processes, revealing a complex regulatory interplay of signaling, metabolic and epigenetic adaptations during CD8 T cell differentiation[4,5]. Upon antigen exposure, these signals ultimately guide fate determination of naïve T cells into either short-lived effector T cells (SLECs) or memory cells[6]. The former mediate primary adaptive immune responses against pathogens through the release of cytotoxic granules and pro-inflammatory cytokines such as interleukin-2 (IL-2) and interferon gamma (IFN-γ)[7,8]. In contrast, long-lived memory cells remain quiescent while patrolling for previously encountered antigens and activate secondary immune responses upon pathogen recognition[9].

Upon activation, effector CD8 T cells must undergo clonal expansion, necessitating as many as 20 replication cycles to generate sufficient daughter cells to mediate organism-wide pathogen clearance[6]. This energetically costly process necessitates the biosynthesis of essential building blocks including the nucleic acids, amino acids, proteins, and lipids required to sustain the proliferative burst and cytokine production underlying the primary adaptive immune response, which requires rapid ATP production[4]. Previous studies of the metabolic cues that regulate CD8 T cell differentiation at the population level suggest that the exit from quiescence is supported by a dramatic metabolic shift from a predominantly oxidative program in naïve cells, fueled by the beta-oxidation of long chain fatty acids (LCFA), to a predominantly glycolytic state in SLECs,

characterized by lactate production in the setting of adequate oxygen tension, known as aerobic glycolysis[10–12]. This metabolic conversion has been hypothesized to permit continued cycling through the pentose phosphate pathway, thereby enabling continued generation of nicotinamide adenine dinucleotide phosphate (NADPH) and other intermediates necessary for anabolic processes, including nucleic acid production and lipid biosynthesis, while also circumventing negative feedback induced by the accumulation of pyruvate and acetyl-CoA[4,13]. Additional feed-forward mechanisms supporting this process include the activity of downstream transcription factors of the phosphoinositide 3-kinase (PI3K) signaling cascade such as hypoxia inducible factor 1 (HIF1α), which mediates the upregulation of nutrient receptors including glucose transporter 1 (Glut1), the main point of entry for glucose into T cells[10].

Meanwhile, the transition to the memory T cell fate is associated with the inhibition of PI3K/mTORC1 signaling and silencing of aerobic glycolysis by AMP-activated protein kinase (AMPK) in favor of mitochondrial biogenesis and fusion[8,14,15,16], which is mediated by peroxisome proliferator-activated receptor gamma coactivator 1-alpha (PGC1α)[11,17]. Interestingly, this regulatory process has been shown to impact chromatin accessibility via both the activity of Ezh2[18,19] and direct histone acetylation and methylation by anaplerotic intermediates of the tricarboxylic acid (TCA) cycle (also known as the citric acid cycle), such as acetyl-coA and alpha ketoglutarate (αKG)[20–22]. This tightly regulated metabolic shift results in an LCFA-fueled oxidative program characterized by increased mitochondrial mass[14]. This property of memory cells has been shown to confer additional oxidative potential known as spare respiratory capacity (SRC), which permits more rapid and potent recall during secondary immune responses[23].

However, while the above reports generated from population-based data suggest that a reciprocal, tightly regulated relationship exists between OXPHOS and glycolysis as well as the signaling cascades that regulate these pathways, the precise interactions of these processes in individual cells, and the transition states through which they pass on the way to their terminally differentiated state, have yet to be elucidated. Simultaneously, considerable progress has been made in defining changes in signaling and effector T cells programs at the single-cell level[24,25]. However, integrating the measurement of metabolism into these studies remains largely unexplored. Many of the regulatory mechanisms that govern cellular metabolism are post-translational and therefore not directly measurable by sequencing[17]. Therefore, to comprehensively assess the coordinated program dictating CD8 T cell fate and function, a single-cell proteomic approach provides unique opportunities.

Mass cytometry, a next-generation advance in flow cytometry, utilizes metal-tagged antibodies to directly measure up to 45 proteins simultaneously in individual cells[26,27]. This approach has permitted broad-spectrum, organism-wide characterization of various aspects of cellular behavior including phenotype, signaling[28], proliferation[29] and chromatin state[30]. Here, we have further adapted this platform to measure expression levels of the enzymes and transporters involved in these crucial metabolic checkpoints. We have integrated direct quantitative evaluation of the signaling cues thought to mediate their function along with markers characterizing CD8 T cell fate and function. In this study we utilize this novel approach to interrogate key inflection points of the CD8 T cell response to *Listeria monocytogenes* infection, a well-characterized model of CD8 T cell differentiation[31].

Results

An integrated mass cytometry-based assay permits high-dimensional analysis of CD8 T cell function at the proteomic level with single-cell resolution

T cell activation requires the coordinated interplay of signaling and metabolic pathways, culminating in the upregulation of rate-limiting enzymes and regulatory switches that ultimately promote cellular differentiation. Since activation-induced mitochondrial fusion and biogenesis is regulated by MAP kinase signaling downstream of the TCR and the co-stimulatory molecules CD28 and 4-1BB[11,32], we measured the phosphorylated forms of the ERK and p38 MAP kinases in addition to the total levels of inhibitor of kB (IκB), which have been found to regulate this process in other cell types[33]. Calcium signaling, triggered by TCR ligation, has also been implicated in this process[34,35]. Therefore, we additionally measured phospho (p)-CREB levels. As co-stimulatory signaling through CD28 has also been heavily implicated in the initial steps promoting aerobic glycolysis via the AKT/PI3K pathway[10,36], we measured the downstream intermediates mTOR, pS6, p4EBP1, and HIF1α (Fig. 1a, Table S1). Signaling through this pathway promotes glucose uptake through the Glut1 receptor and the transcription of glycolytic enzymes[37], including glyceraldehyde-3-phosphate dehydrogenase (GADPH) (Fig. 1b), a critical metabolic switch implicated in glycolytic activity, repression of IFN-γ production[38], and apoptosis[39]. To gain an understanding of how these factors impact progression of pyruvate through the TCA cycle, we evaluated the expression of citrate synthase (CS) (Fig. 1b, Table S1), the first step of the TCA cycle linking this process with glycolysis, which is directly regulated by NAD+/NADH ratio, ADP/ATP ratio and succinyl-coA levels[40]. As branched chain amino acid metabolism has been demonstrated to be critical for effective T cell activation[41], we sought to understand this process by measuring the large neutral amino acid transporter (LAT1)

chaperone CD98 (Fig. 1a, Table S1), a key mediator of the import of these essential nutrients[42–44].

Previous work has described a reciprocal relationship between aerobic glycolysis and OXPHOS fueled by LCFA oxidation, a balance which directly impacts T cell fate and function. Therefore, we sought to understand this regulation at the single-cell level through the measurement of CPT1α, an enzyme that catalyzes the transport of LCFA from the cytoplasm to the mitochondria and that has been previously deemed critical for memory T cell function[23]. Additionally, we measured the mitochondrial trifunctional complex, also known as hydroxyacyl-CoA dehydrogenase (HADHA), which catalyzes the final three steps of LCFA oxidation to acetyl-CoA in the mitochondria[45]. Moreover, we measured key components of the electron transport chain, including cytochrome C (CytoC) and ATP synthase (ATP5a) (Fig. 1b, Table S1). As the role of β-oxidation of medium-chain fatty acids in T cell function has not been extensively evaluated[46], we also measured the expression of medium-chain acyl-CoA dehydrogenase (ACADM), an essential enzyme that catalyzes the initial step of this process (Fig. 1b, Table S1). To gain an understanding of the counterregulatory processes governing OXPHOS activity and overall energy, we queried expression of voltage-dependent ion channel 1 (VDAC1), a critical regulator controlling cytoplasmic-mitochondrial cross-talk (Fig. 1b, Table S1)[39,47].

It has been proposed that the activity of metabolic pathways induces the activity of transcription factors and enzymes such Ezh2, which, along with anaplerotic accumulation of acetyl-CoA and α-KG, has been posited to induce epigenetic changes, directly impacting T cell fate and function[18,21]. Therefore, an assay assessing the role of metabolism in CD8 T cell differentiation ought to reliably and comprehensively assess T cell phenotype and cytotoxicity. We therefore included a full range of well-characterized surface markers and transcription factors that would

allow us to subset T cells into naïve, central memory, effector memory and terminal effector populations by both supervised gating and unsupervised analyses. Finally, to measure the impact on all of these factors on T cell proliferation during clonal expansion, we measured expression of cyclinB1 and Ki67. To assess production of cytotoxic mediators of a productive primary immune response, we measured granzyme B in these subsets of interest (Fig. 1a, Table S1).

Mass cytometry recapitulates previously identified metabolic phenotypes of CD8 T cell differentiation in vitro

In order to query the metabolic program underlying antigen-specific CD8 T cell activation *in vitro,* we first stimulated TCR transgenic OT-1 splenocytes in the presence of their cognate antigen (the SIINFEKL peptide from ovalbumin) and IL-2 for 72 hours. After this initial priming period, antigen was removed, and cells were polarized in IL-2 or IL-7 for an additional 4 days to generate effector (OT-1_{eff}) or central memory cells (OT-1_{mem}), as described previously (Fig. 2a, S1a)[8,23,48]. We analyzed the resulting cells by mass cytometry and real-time metabolic profiling by Seahorse assay (Fig. 2a). In keeping with prior studies[8,23], OT-1_{eff} exhibited marked glycolytic activity at day 7 of activation, as evidenced by robust upregulation of Glut1 and GAPDH (Fig. 2b, S2a), suggestive of active glucose uptake and utilization. As IL-2 has been implicated as a key mediator of Glut1 expression and glycolytic activity, these results are consistent with previous data. Additionally, the expression of markers of the PI3K/mTORC1 pathway, including pS6, p4EBP1 and HIF1α, were likewise elevated in OT1_{eff} (Fig. S1a), consistent with the promotion of aerobic glycolysis. In keeping with previous data linking branched chain amino acid transport with effective effector function[41], CD98 expression was higher in OT1_{eff} relative to OT-1_{mem} (Fig. S1a). In contrast to their effector counterparts, OT-1_{mem} did not demonstrate this glycolytic profile, but instead upregulated CPT1α (Fig. 2b), a well-

characterized metabolic adaptation associated with the CD8 memory T cell phenotype[23]. Polarization with IL-15, another cytokine that promotes memory formation[14,23,49], resulted in similar phenotypic and metabolic profiles compared to IL-7 (Fig. S1a).

Next, we interrogated the expression levels of enzymes involved in OXPHOS in these populations. Consistent with results from mature activated T cells[47,50], OT-1_{eff} also demonstrated higher expression of CytoC, ATP5a, and VDAC1 (Fig. S1a). Seahorse analysis further reinforced these findings. Consistent with a more activated state, OT-1_{eff} exhibited higher baseline extracellular acidification rate (ECAR) (Fig.2c-d, Fig. S1d) and oxygen consumption rate (OCR)[51] (Fig.2c-d, Fig. S1c). However, OT-1_{mem} achieved a higher maximum OCR than baseline (Fig. 2c-d, Fig.S1b-c), therefore demonstrating spare respiratory capacity (SRC), a well-described attribute of memory T cells[14,23]. Taken together, our data support the notion of a metabolically active, highly proliferative terminal effector program supported by aerobic glycolysis and enabled by BCAA metabolism in contrast to a quiescent, predominantly OXPHOS-driven memory program fueled by LCFA oxidation.

Single-cell analysis of antigen-specific CD8 T cell activation in vitro reveals a sequential process of early effector activation

Having validated our approach at the population level, we next sought to further characterize the stepwise, coordinated mechanisms underlying CD8 T cell activation in individual cells. Therefore, we barcoded together and analyzed OT-1 T cells fixed at 0, 6, 12, 24, 36, 48, and 72 hours after peptide stimulation as well at days 5 and 7 of IL-2 or IL-7 polarization by mass cytometry. We performed unsupervised analysis of both functional and phenotypic markers across single cells in the dataset, which we visualized as a force-directed graph (Fig. 2e, Fig. S2, Fig S3). In accordance with both previous studies and our bulk data, cells comprising OT-

1_{eff} at Day 7 (Fig. 2e, Fig. S3) demonstrated a predominantly glycolytic metabolic profile as evidenced by expression of Glut1 and HIF1α. Notably, these makers were already upregulated within 6 hours of stimulation and achieved peak levels by 72 hours (Fig. 2e, Fig. S1a). However, while Glut1 was uniformly expressed within all clusters at these earlier time points, unsupervised analysis at single-cell resolution revealed two proliferative populations expressing the costimulatory molecule ICOS but with distinct patterns of GAPDH expression at 48 hours of activation (Fig. 2e-f). These subsets also exhibited distinct cell signaling states. While the $GAPDH^{hi}$ population exhibited higher levels of pCREB, p4EBP1, and pS6 (Fig. 2g), the $GAPDH^{low}$ population demonstrated repressed IκB levels (Fig. 2g), indicative of increased signaling through the NFκB pathway. Additional metabolic and functional differences between these cells were also discernible: the $GAPDH^{hi}$ cells expressed higher levels of granzyme B and VDAC1, while $GAPDH^{low}$ cells expressed higher levels of CD98 and ATP5a (Fig. 2f-g). This phenomenon was not readily apparent when analyzing results at the population level, underscoring the utility of a high-dimensional, single-cell approach to metabolic analysis. These data suggest that CD8 T cells pass through distinct, intermediate transition points even before polarization into distinct differentiation states.

Single-cell analysis of the CD8 T cell effector program* in vivo *reveals a $CD27^{hi}CD25^{hi}ICOS^{hi}$ transitional effector pool with a unique metabolic profile

To further understand the process of CD8 T cell differentiation in a more physiologic context, we next evaluated the trajectory of the response to acute infection *in vivo*. C57BL/6 mice were infected with *Listeria monocytogenes* expressing whole cytoplasmic ovalbumin (Lm-OVA), a well-characterized model of CD8 T cell differentiation and metabolism[8,14,23]. Splenocytes were harvested daily over the first nine days post-infection for analysis by mass cytometry. We

performed unsupervised analysis by Phenograph clustering on both functional and phenotypic markers across all cells in the dataset[52], which were then visualized as a force-directed graph (Fig. 3a, Fig. S4, Fig. S5a, Fig S6a). This approach revealed 12 clusters of CD8 T cells (Fig. 3a-c), including canonically defined naïve ($CD44^{-}CD62L^{+}$), central memory ($CD44^{+}CD62L^{+}$) and effector memory ($CD44^{+}CD62L^{-}KLRG1^{-}$) subsets present from the onset (Fig. 3a-c, S4a, Fig. S5a-b) to the short-lived effector cells ($CD27^{-}CD44^{+}CD62L^{-}KLRG1^{+}$) emerging at Day 6 post-infection and peaking in frequency by days 7 and 8 post-infection, when this subset is typically studied (Fig. 3b)[14,23,49]. Canonical terminal populations recapitulated prior observations, with the SLEC cluster (c12) demonstrating a more glycolytic profile and markedly lower expression of markers of FAO and OXPHOS, and central memory pools (c2, c3) retaining oxidative marker expression (Fig. 3c-e, Fig. S6a-b). Both terminally differentiated subsets displayed greater metabolic and signaling activity compared to their resting naïve counterparts (c4, c5) (Fig. 3c-e, Fig. S6a-b).

However, in addition to these well-characterized cell subsets, unsupervised high-dimensional analysis also revealed a novel, highly proliferative $CD62L^{low}CD44^{hi}CD27^{hi}ICOS^{hi}$ CD8 T cell pool (c7, c8) with variable expression of KLRG1 that emerged at day 4 post-infection (Fig. 3a-b). These cells achieved their maximum frequency at day 5, when they comprised approximately 30% of the CD8 T cell population, and nearly completely disappeared by day 7 (Fig. 3b, Fig S4). We undertook further phenotypic analysis, which identified the high-affinity IL-2 receptor subunit, CD25, as another surface marker uniquely co-expressed by this population of interest (Fig. S7). As ICOS has been found to signal through the PI3K cascade[53], and IL-2 has been identified as a critical mediator of Glut1 expression[54], we anticipated that this population would be intensely glycolytic. Indeed, this early effector pool appeared highly metabolically active; however, these cells unexpectedly exhibited peak expression of both glycolytic and oxidative markers simultaneously (Fig. 3c-e, S6a-b). Commensurate with this observation, the signaling

program of this population was marked by maximal expression of both pS6 and pCREB as well as degradation of IκB, signifying simultaneous activity of both the PI3K/mTORC1 and NFκB pathways (Fig. 3c-e, S6a-b). Notably, in contrast to their SLEC and memory counterparts, this transitional subset appeared poised to utilize both LCFA and BCAA for energy production based on the expression of both CD98 and CPT1α (Fig. 3c-e, S6a-b). These cells appeared to be antigen specific, as adoptively transferred OT-1 T cells also transiently upregulate these surface markers with the same kinetics (Fig. 3f). Given the transience and highly active metabolic phenotype of this newly identified population, we hypothesized that these cells represented a novel transitional state of T cell differentiation and sought to further characterize their function and behavior.

The CD27^{hi}CD25^{hi}ICOS^{hi} transitional population demonstrates peak glycolytic activity and increased mitochondrial activity and mass during the effector phase

Since the CD27^{hi}CD25^{hi}ICOS^{hi} effector subset was distinguished by simultaneously elevated levels of glycolytic and oxidative enzymes, we posited that this expression profile would translate to greater metabolic activity along these pathways when compared to their SLEC counterparts. To assess real-time bioenergetic flux through oxidative and glycolytic pathways in these subsets of interest, we sorted naïve (CD62L^{hi}CD44^{low}KLRG1^{low}CD25^{lo}), transitional effectors (CD62L^{low}CD44^{hi}CD25^{hi}) at day 5 post-infection, and SLECs (CD62L^{low}CD44^{hi}KLRG1^{hi}CD25^{low}) at day 8 post-infection (Fig. S8) for analysis by Seahorse assay. Baseline and maximal OCR did not significantly differ between the SLEC and naive pools as described previously[23] (Fig. 4a-b). However, SLECs demonstrated significantly higher baseline and maximum ECAR compared to their naïve counterparts (Fig.4c), confirming a predominantly glycolytic program driving the terminal effector state *in vivo*.

In accordance with their enzymatic expression profile by mass cytometry, the CD27^{hi}CD25^{hi}ICOS^{hi} transitional subset exhibited significantly higher basal and maximal glycolytic and oxidative activity compared to both the SLEC and naïve pools (Fig. 4a-c). As we noted maximal expression of CPT1α and electron transport complexes by the transitional effector pool, we hypothesized that that this population would possess SRC, in keeping with previous reports studying memory T cells that upregulate these enzymes[23]. Indeed, while neither the naïve or SLEC pools were capable of surpassing their baseline OCR upon FCCP administration, the OCR of the CD27^{hi}CD25^{hi}ICOS^{hi} effector subset nearly doubled (Fig. 4a-b). As SRC has been associated with greater mitochondrial mass[14], we sought to quantify the mitochondrial content of this novel subset. Splenocytes were harvested from animals at days 5 and 8 of LmOVA infection, stained with MitoTracker Deep Red, a fluorescent dye specific for the mitochondrial outer membrane, and analyzed by flow cytometry. Consistent with our mass cytometry and Seahorse data, the CD27^{hi}CD25^{hi}ICOS^{hi} effector subset contained significantly more mitochondrial mass than the SLEC or naïve pools based on MitoTracker staining (Fig. 4d). Overall, these observations confirmed the unique, simultaneously oxidative and glycolytic profile of the CD27^{hi}CD25^{hi}ICOS^{hi} transitional population.

The CD27^{hi}CD25^{hi}ICOS^{hi} transitional pool exhibits proliferative and cytotoxic capacity and gives rise to both effector memory and SLEC cells

As we hypothesized that these cells represented a novel transitional state of T cell differentiation, we sought to further understand their developmental trajectory. We therefore sorted CD27^{hi}CD25^{hi}ICOS^{hi} transitional effectors and SLECs from CD45.1^{+} animals at days 5 and 8 post-infection (Fig. S8) and transferred them into infected CD45.2^{+} hosts, which were then sacrificed four days later (Fig. 5a). Given the elevated expression of CyclinB1 and Ki67

exhibited by the CD27^{hi}CD25^{hi}ICOS^{hi} subset (Fig. 3c, Fig. S6a-b), we hypothesized that this population would demonstrate greater expansion upon adoptive transfer. Indeed, a significantly higher number of CD45.1^{+} cells were detected in hosts receiving transitional cells compared to SLECs (Fig. 5b). These daughter cells retained a more proliferative and cytotoxic phenotype, with higher levels of Ki67 and granzyme B expression compared to cells derived from SLECs (Fig. 5c), though they had downregulated CD25 and ICOS by this time point (Fig. 5d). Consistent with a transient burst of metabolic activity, these cells exhibited lower expression of both glycolytic and oxidative markers compared to the CD27^{hi}CD25^{hi}ICOS^{hi} cells found at day 5 post-infection, but they retained greater levels of these enzymes compared to the transferred SLECs (Fig. 5d). In keeping with a terminally differentiated state, SLECs retained their phenotype upon adoptive transfer (Fig. 5e). However, the CD27^{hi}CD25^{hi}ICOS^{hi} subset demonstrated multiple differentiation states: most daughter cells upregulated KLRG1 and adopted a SLEC phenotype, but a significant fraction of cells assumed a memory phenotype, expressing CD27 but not KLRG1 (Fig. 5e).

To determine the differentiation state of these transferred cells in an unsupervised manner, we adapted the Scaffold maps algorithm[55] to plot each individual cell in relation to canonically defined reference nodes based on phenotypic and functional marker expression (Fig. 5f). Consistent with our manual gating, the transitional cells had differentiated by day 9 post-infection, and most cells were categorized as SLEC or effector memory cells. Taken together, these data indicate that, shortly after activation, CD8 T cells pass through a highly metabolically active, simultaneously glycolytic and oxidative state further characterized by CD25 and ICOS co-expression. During differentiation, silencing of these pathways takes place coordinate with determination of short-lived or memory fates early in the course of an adaptive immune response.

Discussion

Mass cytometry by time-of-flight permits broad-spectrum characterization of immune responses across multiple systems in healthy and diseased states[56]. To date, this approach has been used to query the phenotypic and signaling adaptations undertaken by cells during differentiation[57,58]. However, until now, the coordinated downstream metabolic cues supporting these programs have remained incompletely understood at the single-cell level. Here, we directly measured the expression levels of essential nutrient receptors, enzymes, signaling intermediates, and markers of cellular differentiation and effector function at the proteomic level. This allowed us to more thoroughly characterize CD8 T cell responses during acute infection, capturing a novel transition point in CD8 T cell activation.

While previous models of the naïve-to-effector transition based on bulk data have proposed a process in which OXPHOS is repressed to promote aerobic glycolysis[10,59], it has recently been reported that effector T cells may utilize oxidative phosphorylation *in vivo*[60]. Our data unify these observations, supporting a coordinated program in which these two pathways are maintained simultaneously during an earlier stage of T cell activation. Notably, high rates of proliferation were also an attribute of cells at this time point. As glutaminolysis has been shown to be essential for the generation of anaplerotic substrates of the TCA cycle, and while this has been linked mTOR mediated metabolic reprogramming[10,61], it is also possible that these intermediates are in part responsible for the observed maintenance of OXPHOS in the transitional pool. Additionally, it has been observed that effector T cells engage in more active LCFA uptake than their memory cell counterparts, which instead have been shown to mobilize these substrates from lysosomal triglycerides[49]. It is therefore feasible that fatty acid uptake may provide additional substrate for OXPHOS early in the course of T cell activation. Additional studies

modulating nutrient uptake in this novel subset will be required to more thoroughly characterize the relative contribution of each of these pathways to their proliferation and cytotoxicity.

The CD27^{hi}CD25^{hi}ICOS^{hi} subset emerges at day 4 post-infection *in vivo*, and notably our data reveal an analogous population at 48 hours of stimulation *in vitro*. This consistent timing across both contexts suggests a potential role for co-stimulation during CD8 T cell priming in this potentiation of this mitochondrial activity. Notably 4-1BB ligation during co-stimulation has been shown to induce mitochondrial fusion via TRAF2-mediated signaling through p38 and PGC1α[11,32]. Similarly, CD28 ligation been demonstrated to induce CPT1α expression *in vitro*[51]. Whether these signals potentiate the observed spare respiratory capacity and increased mitochondrial mass in the transitional pool will be important to determine. As Drp1 mediated mitochondrial fission has been described in effector pools during metabolic reprogramming to the aerobic glycolytic program[14], it is possible that the absence of co-stimulation and loss of IL-2 signaling upon pathogen clearance may result in mitophagy and/or mitochondrial fission, repressing oxidative activity as observed in terminal effector subsets. Further studies evaluating the mitochondrial dynamics of this novel transitional subset will be necessary to address this question.

Our approach to metabolic profiling by mass cytometry affords investigators the opportunity to functionally characterize the fate trajectories of rare cellular populations, such as antigen-specific T cells. These cells would be otherwise difficult to analyze by the current standard metabolomics assays due to the often prohibitively large number of cells and extensive processing and ex vivo culture techniques required for these studies[62,63]. Here, we were able to characterize the metabolic, signaling and phenotypic progeny of adoptively transferred cells with single-cell resolution. This approach revealed a diversification during CD8 T cell differentiation in the context of acute infection, with a highly metabolically active and proliferative transitional

subset arising early in the course of infection that gave rise to cells with both memory and terminal effector phenotypes. The emergence of this transitional cell subset with co-stimulatory marker expression may support evidence from previous studies suggesting that CD8 T cell differentiation may be determined early in the course of activation[29,64]. Our findings therefore seem to indicate that attempts to manipulate metabolic pathways to modulate immune responses would be most effective during T cell priming rather than during the effector phase.

As the importance of metabolism to immune cell fate and function is increasingly appreciated, methods to evaluate these pathways in models of productive and dysregulated immune responses will be critical. The approach presented here may be adapted to any cell type of interest, including both immune cells and non-immune cells, such as interacting epithelial tissues and a wide variety of tumor histologies. This novel method should enable investigators to query the functional programs underlying the development of the full spectrum of immune cell lineages and their compromised state in the context of autoimmunity or malignancy. Additionally, integrated functional analysis of rare cellular subsets will permit simultaneous evaluation of the effects of various treatments on populations such as tumor infiltrating lymphocytes or neoantigen-specific T cells. Finally, this antibody-based approach may be further adapted for highly multiplexed imaging approaches such as multiplexed ion beam imaging (MIBI)[65] or imaging mass cytometry (IMC)[66] to enable direct visualization of spatial localization and its relation to cellular metabolism in a variety of contexts.

Acknowledgements:

We would like to thank the members of the Spitzer lab, Vinh Ngyuen, Stanley Tamaki, Sagar Bapat, Adil Daud, Lawrence Fong, Andrei Goga, Rushika Perera for their experimental contributions and helpful discussions. Listeria monocytogenes strain 10403s expressing OVA (Lm-OVA) was kindly provided by Shomyseh Sanjabi (UCSF). We acknowledge the Parnassus Flow Cytomtery Core Facility supported in part by Grants NIH P30 DK063720, NIH S10 1S10OD018040-01, NIH S10 1S10OD018040-01 and NIH S10 1S10OD021822-01.

Recombinant human IL-2 (IL-2; TECIN (Teceleukin)) was provided by the National Cancer Institute.

This work was supported by NIH grant DP5 OD023056 to MHS. LSL was supported by Conquer Cancer Foundation Young Investigator Award grant CA-0122026. MHS is a Chan Zuckerberg Biohub investigator and a Parker Institute for Cancer Immunotherapy investigator.

Author Contributions:

L.S.L., J.C.R., and M.H.S. conceptualized this study and designed experiments. L.S.L, K.J.H. D.M.M., I.T. and D.C.C. performed experiments. L.S.L, K.J.H., and M.H.S. performed high-dimensional data analysis. L.S.L. and M.H.S. wrote the manuscript. M.H.S. supervised the study.

Competing Interest Statement:

M.H.S. has been a paid consultant for Five Prime Therapeutics, Ono Pharmaceutical and January, Inc. and has received funding support from Roche/Genentech, Pfizer, Valitor Inc., and Bristol-Myers Squibb. J.C.R. is a founder and member of the scientific advisory board of Sitryx Therapeutics, and member of the scientific advisory boards of Caribou Biosciences, Istesso Ltd, has received research funding from Kadmon, Incyte, Tempest, and Calithera, and received honorarium from Merck and Pfizer.

References

1. Buck, M. D., Sowell, R. T., Kaech, S. M. & Pearce, E. L. Metabolic Instruction of Immunity. *Cell* **169**, 570–586 (2017).
2. Restifo, N. P., Dudley, M. E. & Rosenberg, S. A. Adoptive immunotherapy for cancer: harnessing the T cell response. *Nat. Rev. Immunol.* **12**, 269–281 (2012).
3. Callahan, M. K., Postow, M. A. & Wolchok, J. D. Targeting T Cell Co-receptors for Cancer Therapy. *Immunity* **44**, 1069–1078 (2016).
4. Zhang, L. & Romero, P. Metabolic Control of CD8 + T Cell Fate Decisions and Antitumor Immunity. *Trends Mol. Med.* **24**, (2017).
5. Olenchock, B. A., Rathmell, J. C. & Vander Heiden, M. G. Biochemical Underpinnings of Immune Cell Metabolic Phenotypes. *Immunity* **46**, 703–713 (2017).
6. Badovinac, V. P., Haring, J. S. & Harty, J. T. Initial T Cell Receptor Transgenic Cell Precursor Frequency Dictates Critical Aspects of the CD8+ T Cell Response to Infection. *Immunity* (2007) doi:10.1016/j.immuni.2007.04.013.
7. Araki, K. *et al.* HHS Public Access. **460**, 108–112 (2010).
8. Pearce, E. L. *et al.* Enhancing CD8 T-cell memory by modulating fatty acid metabolism. *Nature* **460**, 103–107 (2009).
9. Gerriets, V. A. & Rathmell, J. C. Metabolic pathways in T cell fate and function. *Trends Immunol.* **33**, 168–173 (2012).
10. Wang, R. *et al.* The Transcription Factor Myc Controls Metabolic Reprogramming upon T Lymphocyte Activation. *Immunity* (2011) doi:10.1016/j.immuni.2011.09.021.
11. Menk, A. V. *et al.* 4-1BB costimulation induces T cell mitochondrial function and biogenesis enabling cancer immunotherapeutic responses. *J. Exp. Med.* **215**, 1091–1100 (2018).
12. Menk, A. V. *et al.* Early TCR Signaling Induces Rapid Aerobic Glycolysis Enabling

Distinct Acute T Cell Effector Functions. *Cell Rep.* **22**, 1509–1521 (2018).
13. Lee, J. *et al.* Regulator of fatty acid metabolism, acetyl coenzyme a carboxylase 1, controls T cell immunity. *J. Immunol.* **192**, 3190–3199 (2014).
14. Buck, M. D. D. *et al.* Mitochondrial Dynamics Controls T Cell Fate through Metabolic Programming. *Cell* **166**, 63–76 (2016).
15. Borges da Silva, H. *et al.* The purinergic receptor P2RX7 directs metabolic fitness of long-lived memory CD8(+) T cells. *Nature* **559**, 264–268 (2018).
16. D'Souza, A. D., Parikh, N., Kaech, S. M. & Shadel, G. S. Convergence of multiple signaling pathways is required to coordinately up-regulate mtDNA and mitochondrial biogenesis during T cell activation. *Mitochondrion* **7**, 374–385 (2007).
17. Andrejeva, G. & Rathmell, J. C. Similarities and Distinctions of Cancer and Immune Metabolism in Inflammation and Tumors. *Cell Metab.* **26**, 49–70 (2017).
18. Gray, S. M., Amezquita, R. A., Guan, T., Kleinstein, S. H. & Kaech, S. M. Polycomb Repressive Complex 2-Mediated Chromatin Repression Guides Effector CD8+ T Cell Terminal Differentiation and Loss of Multipotency. *Immunity* (2017) doi:10.1016/j.immuni.2017.03.012.
19. Gray, S. M., Amezquita, R. A., Guan, T., Kleinstein, S. H. & Kaech, S. M. Polycomb Repressive Complex 2-Mediated Chromatin Repression Guides Effector CD8+ T Cell Terminal Differentiation and Loss of Multipotency. *Immunity* **46**, 596–608 (2017).
20. Chisolm, D. A. & Weinmann, A. S. Connections Between Metabolism and Epigenetics in Programming Cellular Differentiation. *Annu. Rev. Immunol.* **36**, 221–246 (2018).
21. Chisolm, D. A. *et al.* CCCTC-Binding Factor Translates Interleukin 2- and α-Ketoglutarate-Sensitive Metabolic Changes in T Cells into Context-Dependent Gene Programs. *Immunity* **47**, 251-267.e7 (2017).
22. Peng, M. *et al.* Aerobic glycolysis promotes T helper 1 cell differentiation through an epigenetic mechanism. *Science (80-.).* **354**, 481 LP – 484 (2016).
23. van der Windt, G. J. W. *et al.* Mitochondrial Respiratory Capacity Is a Critical Regulator of CD8 + T Cell Memory Development. *Immunity* (2012) doi:10.1016/j.immuni.2011.12.007.
24. Mingueneau, M. *et al.* Single-cell mass cytometry of TCR signaling: Amplification of small initial differences results in low ERK activation in NOD mice. *Proc. Natl. Acad. Sci.* **111**, 16466 LP – 16471 (2014).
25. Krishnaswamy, S. *et al.* Conditional density-based analysis of T cell signaling in single-cell data. *Science (80-.).* **346**, 1250689 (2014).
26. Bandura, D. R. *et al.* Mass Cytometry: Technique for Real Time Single Cell Multitarget Immunoassay Based on Inductively Coupled Plasma Time-of-Flight Mass Spectrometry. *Anal. Chem.* **81**, 6813–6822 (2009).
27. Newell, E. W., Sigal, N., Bendall, S. C., Nolan, G. P. & Davis, M. M. Cytometry by Time-of-Flight Shows Combinatorial Cytokine Expression and Virus-Specific Cell Niches within a Continuum of CD8 + T Cell Phenotypes. *Immunity* **36**, 142–152 (2012).
28. Bodenmiller, B. *et al.* Multiplexed mass cytometry profiling of cellular states perturbed by small-molecule regulators. *Nat. Biotechnol.* **30**, 858–867 (2012).
29. Good, Z. *et al.* Proliferation tracing with single-cell mass cytometry optimizes generation of stem cell memory-like T cells. *Nat. Biotechnol.* **37**, 259–266 (2019).
30. Cheung, P. *et al.* Single-Cell Chromatin Modification Profiling Reveals Increased Epigenetic Variations with Aging. *Cell* **173**, 1385-1397.e14 (2018).
31. MCGREGOR, D. D., KOSTER, F. T. & MACKANESS, G. B. Biological Sciences: The Short Lived Small Lymphocyte as a Mediator of Cellular Immunity. *Nature* **228**, 855–856 (1970).
32. Teijeira, A. *et al.* Mitochondrial morphological and functional reprogramming following CD137 (4-1BB) Costimulation. *Cancer Immunol. Res.* **6**, 798–811 (2018).
33. Laforge, M. *et al.* NF-κB pathway controls mitochondrial dynamics. *Cell Death Differ.* **23**,

89–98 (2016).
34. Feske, S. Calcium signalling in lymphocyte activation and disease. *Nat. Rev. Immunol.* **7**, 690–702 (2007).
35. Fracchia, K. M., Pai, C. Y. & Walsh, C. M. Modulation of T Cell Metabolism and Function through Calcium Signaling. *Front. Immunol.* **4**, 1–11 (2013).
36. Pollizzi, K. N. *et al.* mTORC1 and mTORC2 selectively regulate CD8+ T cell differentiation. *J. Clin. Invest.* **125**, 2090–2108 (2015).
37. Dennis, M. K. *et al.* Postranscriptional control of T cell effector function by aerobic glycolysis. *Cell* **127**, 358–366 (2012).
38. Chang, C. H. *et al.* XPosttranscriptional control of T cell effector function by aerobic glycolysis. *Cell* **153**, 1239 (2013).
39. Tarze, A. *et al.* GAPDH, a novel regulator of the pro-apoptotic mitochondrial membrane permeabilization. *Oncogene* **26**, 2606–2620 (2007).
40. Wiegand, G. & Remington, S. J. CITRATE SYNTHASE: Structure, Control, and Mechanism. *Annu. Rev. Biophys. Biophys. Chem.* **15**, 97–117 (1986).
41. Ren, W. *et al.* Amino-acid transporters in T-cell activation and differentiation. *Cell Death Dis.* **8**, 1–9 (2017).
42. Hayashi, K., Jutabha, P., Endou, H., Sagara, H. & Anzai, N. LAT1 Is a Critical Transporter of Essential Amino Acids for Immune Reactions in Activated Human T Cells. *J. Immunol.* **191**, 4080 LP – 4085 (2013).
43. Nii, T. *et al.* amino acid transporter LAT1 during T-cell activation. *Reactions* **704**, 693–704 (2001).
44. Sinclair, L. V *et al.* Control of amino-acid transport by antigen receptors coordinates the metabolic reprogramming essential for T cell differentiation. *Nat. Immunol.* **14**, 500–508 (2013).
45. Carpenter, K., Pollitt, R. J. & Middleton, B. Human liver long-chain 3-hydroxyacyl-coenzyme a dehydrogenase is a multifunctional membrane-bound beta-oxidation enzyme of mitochondria. *Biochem. Biophys. Res. Commun.* **183**, 443–448 (1992).
46. Howie, D., Ten Bokum, A., Necula, A. S., Cobbold, S. P. & Waldmann, H. The Role of Lipid Metabolism in T Lymphocyte Differentiation and Survival . *Frontiers in Immunology* vol. 8 1949 (2018).
47. Cunningham, C. A., Hoppins, S. & Fink, P. J. Cutting Edge: Glycolytic Metabolism and Mitochondrial Metabolism Are Uncoupled in Antigen-Activated CD8 + Recent Thymic Emigrants . *J. Immunol.* **201**, 1627–1632 (2018).
48. Carrio, R., Bathe, O. F. & Malek, T. R. Initial Antigen Encounter Programs CD8 + T Cells Competent to Develop into Memory Cells That Are Activated in an Antigen-Free, IL-7- and IL-15-Rich Environment . *J. Immunol.* **172**, 7315–7323 (2004).
49. Sullivan, D. O. *et al.* Memory CD8+ T Cells use cell intrinsic lipolysis. *Immunity* **41**, 75–88 (2014).
50. Tarasenko, T. N. *et al.* Cytochrome c Oxidase Activity Is a Metabolic Checkpoint that Regulates Cell Fate Decisions During T Cell Activation and Differentiation. *Cell Metab.* **25**, 1254-1268.e7 (2017).
51. Klein Geltink, R. I. *et al.* Mitochondrial Priming by CD28. *Cell* **171**, 385-397.e11 (2017).
52. Levine, J. H. *et al.* Data-Driven Phenotypic Dissection of AML Reveals Progenitor-like Cells that Correlate with Prognosis. *Cell* **162**, 184–197 (2015).
53. Zeng, H. *et al.* mTORC1 and mTORC2 Kinase Signaling and Glucose Metabolism Drive Follicular Helper T Cell Differentiation. *Immunity* **45**, 540–554 (2016).
54. Macintyre, A. N. *et al.* The glucose transporter Glut1 is selectively essential for CD4 T cell activation and effector function. *Cell Metab.* (2014) doi:10.1016/j.cmet.2014.05.004.
55. Spitzer, M. H. *et al.* An interactive reference framework for modeling a dynamic immune system. *Science (80-.).* **349**, 1259425 (2015).

56. Spitzer, M. H. & Nolan, G. P. Mass Cytometry: Single Cells, Many Features. *Cell* **165**, 780–791 (2016).
57. Zunder, E. R., Lujan, E., Goltsev, Y., Wernig, M. & Nolan, G. P. A continuous molecular roadmap to iPSC reprogramming through progression analysis of single-cell mass cytometry. *Cell Stem Cell* **16**, 323–337 (2015).
58. Bendall, S. C. *et al.* Single-cell trajectory detection uncovers progression and regulatory coordination in human b cell development. *Cell* **157**, 714–725 (2014).
59. Sukumar, M. *et al.* Inhibiting glycolytic metabolism enhances CD8+ T cell memory and antitumor function. *J. Clin. Invest.* **123**, 4479–4488 (2013).
60. Ma, E. H. *et al.* Metabolic Profiling Using Stable Isotope Tracing Reveals Distinct Patterns of Glucose Utilization by Physiologically Activated CD8+ T Cells. *Immunity* **51**, 856-870.e5 (2019).
61. Durán, R. V. *et al.* Glutaminolysis Activates Rag-mTORC1 Signaling. *Mol. Cell* **47**, 349–358 (2012).
62. Cantor, J. R. *et al.* Physiologic Medium Rewires Cellular Metabolism and Reveals Uric Acid as an Endogenous Inhibitor of UMP Synthase. *Cell* **169**, 258-272.e17 (2017).
63. van der Windt, G. J. W., Chang, C.-H. & Pearce, E. L. Measuring Bioenergetics in T Cells Using a Seahorse Extracellular Flux Analyzer. *Curr. Protoc. Immunol.* **113**, 3.16B.1-3.16B.14 (2016).
64. Chen, Y. H. *et al.* Asymmetric PI3K Activity in Lymphocytes Organized by a PI3K-Mediated Polarity Pathway. *Cell Rep.* **22**, 860–868 (2018).
65. Angelo, M. *et al.* Multiplexed ion beam imaging of human breast tumors. *Nat. Med.* **20**, 436–442 (2014).
66. Giesen, C. *et al.* Highly multiplexed imaging of tumor tissues with subcellular resolution by mass cytometry. *Nat. Methods* **11**, 417–422 (2014).

Figure Legends

Figure 1

Querying the integrated functional program of CD8 T cell activation. Panel schematic depicting signaling, metabolic, effector and phenotypic targets interrogated by mass cytometry. Cell surface, cytosolic and nuclear markers are depicted in **(a)** and mitochondrial markers are denoted in **(b)**. Markers directly measured by mass cytometry are demarcated by an asterisk (*).

Figure 2

Assessing the integrated functional program of antigen specific CD8 T cell activation *in vitro*. (a) OT-1 transgenic CD8 T cells were stimulated with cognate peptide (SIINFEKL) in the presence of IL-2 (100U/ml) for 72 hours, followed by 3 washes to remove antigen and polarization in IL-2 or IL-7 (both 10ng/mL) to generate OT-1_{eff} or OT-1_{mem}. Samples were fixed for mass cytometry at all time points depicted, and cells were harvested at Day 7 for Seahorse assay analysis by Mitochondrial Stress Test. **(b)** Mass cytometry expression profiles of Day 7 $OT1_{eff}$ and $OT1_{mem}$ for key metabolic enzymes as depicted by histograms. **(c)** Oxygen consumption rate (OCR) tracings of Day 7 $OT1_{eff}$ and $OT1_{mem}$ by Mitochondrial Stress Test. **(d)** Basal and maximal OCR and ECAR of Day 7 $OT1_{eff}$ and $OT1_{mem}$ by Seahorse Assay depicted in bar plots and with significance analysis by student's t-test ($p<.001$ ****). Error bars represent SEM. **(e)** Force-directed graph depicting pooled CD8 T cells from all time points of stimulation analyzed by mass cytometry highlighting the dissociation between Glut1 and GAPDH expression patterns in individual cells at 48 hrs post-stimulation. **(f)** Glut1 and GAPDH dissociation as visualized in the primary data depicted by biaxial plots. **(g)** Expression levels of

signaling and metabolic markers as measured by mass cytometry depicted in by histograms. Data are representative of 3 independent experiments.

Figure 3

Single-cell analysis of the CD8 T cell effector program *in vivo*. (a) Pooled CD8 T cells from mice at days 0 to 9 of Lm-OVA infection (n=2-3 mice per time point) clustered by Phenograph and visualized by a force-directed graph. **(b)** Cluster proportion by time point. **(c)** Functional and phenotypic median expression profiles for each CD8 T cell cluster**. (d)** Force-directed graphs for individual oxidative, glycolytic and key signaling marker expression. **(e)** Individual cluster expression profiles for key metabolic enzymes and signaling mediators. **(f)** Percentages of $CD25^{hi}$ endogenous $CD45.2^{+}$ and $CD45.1^{+}$ OT-1 adoptively transferred CD8 T cells at days 4 and 10 p.i. as measured by flow cytometry.

Figure 4

Evaluating glycolytic and oxidative capacity of the $CD27^{hi}CD25^{hi}ICOS^{hi}$ transitional subset. (a) CD8 T cell subsets of interest including, naïve cells ($CD62L^{hi}CD44^{low}KLRG1^{low}CD25^{low}$) Transitional effectors ($CD62L^{low}CD44^{hi}KLRG1^{var}CD25^{hi}$) and SLECs ($CD62L^{low}CD44^{hi}KLRG1^{hi}CD25^{low}$) were sorted at days 5 and 8 p.i. and analyzed by Mitochondrial Stress Test (n=5 mice per time point). OCR tracings. **(b)** Basal and maximal OCR readings obtained upon FCCP administration. **(c)** Basal and maximal ECAR readings measured upon oligomycin administration**. (d)** MitoTracker signal in each subset (n=5 mice per subset). Significance analysis by paired two-tailed student's t-test ($p<0.05$ *, $p<0.01$ **). Error bars represent SEM. Data are representative of at least 2 independent experiments.

Figure 5

Identifying the fate trajectory of the transitional effector pool. (a) Transitional effectors ($CD62L^{low}CD44^{hi}KLRG1^{var}CD25^{hi}$) or SLECs ($CD62L^{low}CD44^{hi}KLRG1^{hi}CD25^{low}$) were sorted from $CD45.1^{+}$ mice at Days 5 and 8 p.i. respectively (and transferred into infected $CD45.2^{+}$ hosts at Day 5 p.i (n=2 per group) and sacrificed 4 days later for analysis by mass cytometry. **(b)** Percentages of CD45.1 cells from SLEC or transitional donors at time of sacrifice (significance analysis by paired two-tailed student's t-test with $p<0.05$ *, $p<0.01$ **). Error bars represent SEM. **(c)** Expression profile of Ki67 and Granzyme B of transferred SLEC and transitional cells at time of sacrifice. **(d)** Metabolic and signaling marker profiles of transferred SLEC and transitional cells are represented in violin plots. **I** Differentiation state of the transitional subset determined by CD44 and KLRG1 expression at day 9 p.i. **(f)** Single-cell Scaffold map depicting differentiation state of individual cells represented by blue nodes in reference to canonically defined landmark nodes in red. Data are representative of at least 2 independent experiments.

Figure S1

Assessing the integrated functional program of antigen specific CD8 T cell activation in vitro. (a) OT-1 transgenic CD8 T cells were stimulated with cognate peptide (SIINFEKL) in the presence of IL-2 (100U/ml) for 72 hours, followed by 3 washes to remove antigen and polarization in IL-2, IL-7 or IL-15 (all 10ng/mL) to generate $OT\text{-}1_{eff}$ or $OT\text{-}1_{mem}$. Samples were fixed for mass cytometry at all time points depicted and cells were harvested at Day 7 for Seahorse assay analysis by Mitochondrial Stress Test. Mass cytometry expression data for key metabolic, signaling and effector markers of interest**. (b)** OCR tracings as quantified by Seahorse. **(c)** Basal and maximal OCR readings and **(d)** basal and maximal ECAR readings as quanfied by Seahorse. Significance analysis by paired two-tailed student's t-test ($p<0.05$ *,

p<0.01 **). Error bars represent SEM. Data are representative of at least 2 independent experiments.

Figure S2

Assessing the integrated functional program of antigen specific CD8 T cell activation in vitro with single-cell resolution. OT-1 transgenic CD8 T cells were stimulated with cognate peptide (SIINFEKL) in the presence of IL-2 (100U/ml) for 72 hours, followed by 3 washes to remove antigen and polarization in IL-2, IL-7 or IL-15 (all 10ng/mL) to generate OT-1_{eff} or OT-1_{mem}. Samples were fixed for mass cytometry at all time points. Force-directed graphs for individual phenotypic expression are depicted.

Figure S3

Assessing the integrated functional program of antigen specific CD8 T cell activation in vitro with single-cell resolution. OT-1 transgenic CD8 T cells were stimulated with cognate peptide (SIINFEKL) in the presence of IL-2 (100U/ml) for 72 hours, followed by 3 washes to remove antigen and polarization in IL-2, IL-7 or IL-15 (all 10ng/mL) to generate OT-1_{eff} or OT-1_{mem}. Samples were fixed for mass cytometry at all time points. Force-directed graphs for individual oxidative, glycolytic, and signaling marker expression are depicted.

Figure S4

Single-cell analysis of the CD8 T cell effector program in vivo. Pooled CD8 T cells from mice at days 0 to 9 of Lm-OVA infection (n=2-3 mice per time point) clustered by Phenograph and visualized by a force-directed graph annotated by time point.

Figure S5

Single-cell phenotypic analysis of the CD8 T cell effector program in vivo. (a) Pooled CD8 T cells from mice at days 0 to 9 of Lm-OVA infection (n=2-3 mice per time point) clustered by Phenograph and visualized by a force-directed graphs. Force-directed graphs of single-cell expression profiles of individual phenotypic markers are depicted. **(b)** Cluster expression profiles for individual phenotypic markers.

Figure S6

Single-cell functional analysis of the CD8 T cell effector program in vivo. (a) Pooled CD8 T cells from mice at days 0 to 9 of Lm-OVA infection (n=2-3 mice per time point) clustered by Phenograph and visualized by a force-directed graphs. Force-directed graphs of single-cell expression profiles of individual functional markers are depicted. **(b)** Cluster expression profiles for individual functional markers.

Figure S7

Identification of a transitional effector pool with co-expression of ICOS and CD25. Biaxial plots depicting mass cytometry expression data for CD25 and ICOS identifies a double positive population at day 5 of infection.

Figure S8

Isolating CD8 T cell subsets for orthogonal validation of mass cytometry data and fate mapping. Sorting strategy for isolation of naïve ($CD62L^{hi}CD44^{low}KLRG1^{low}CD25^{lo}$), transitional effectors ($CD62L^{low}CD44^{hi}KLRG1^{var}CD25^{hi}$) at day 5 post-infection and SLECs ($CD62L^{low}CD44^{hi}KLRG1^{hi}CD25^{low}$) and day 8 post-infection is depicted by biaxial plots.

Table S1

A mass cytometry panel targeting functional and phenotypic aspects of T cell differentiation. Antibodies used in this study and their specifications are depicted in the table.

Methods

EXPERIMENTAL MODEL DETAILS

Animals

All mice were housed in an American Association for the Accreditation of Laboratory Animal Care–accredited animal facility and maintained in specific pathogen-free conditions. Animal experiments were approved and conducted in accordance with AN157618. Wild-type female BALB/c or C57BL/6 mice between 8-10 weeks old were purchased from The Jackson Laboratory and housed at our facility. TCR Transgenic OT-I CD45.1 mice and heterozygous CD45.2/CD45.1 mice were bred at our facility. Animals were housed under standard SPF conditions with typical light/dark cycles and standard chow.

Infectious Agents

Listeria monocytogenes strain 10403s expressing OVA (Lm-OVA) was kindly provided by Shomyseh Sanjabi (UCSF). Lm-OVA stocks frozen at −80 C were grown overnight at 37 C in BHI broth supplemented with 5 ug/ml Erythromycin (Bio Basic, Amherst, New York). Then, overnight cultures were sub-cultured by diluting into fresh BHI broth supplemented with 5 ug/ml Erythromycin and grown for 4 hours. Bacteria CFU was then quantified by measuring optical density at 600 nm. Bacteria were then diluted to 5×104 CFU / 100µl in sterile PBS and 100 µl was injected per mouse i.v. via the retroorbital vein.

METHODS DETAILS

Mass Cytometry Antibodies

All mass cytometry antibodies and concentrations used for analysis can be found in Table S1. Primary conjugates of mass cytometry antibodies were prepared using the MaxPAR antibody conjugation kit (Fluidigm, South San Francisco, CA) according to the manufacturer's recommended protocol. Following labeling, antibodies were diluted in Candor PBS Antibody Stabilization solution (Candor Bioscience GmbH, Wangen, Germany) supplemented with 0.02% NaN3 to between 0.1 and 0.3 mg/mL and stored long-term at 4°C. Each antibody clone and lot was titrated to optimal staining concentrations using primary murine samples.

In vitro OT1 Stimulation and Polarization

OT-1 polarizations were carried out as previously described (Carrio et al, 2004). Briefly, splenocytes from OT-1 mice were cultured at $1*10^6$ cells/mL in 24 well-plates of complete RPMI (UCSF Media Core facility) supplemented with 10% FBS (Omega Scientific, Tarzana, California), 100U/mL penicillin-streptomycin (Fisher Scientific, Hampton, New Hampshire), 2mM L-glutamine (Sigma-Aldrich, St. Louis, Missouri) and 50µM β-mecaptoethanol (Thermo Fisher Scientific, Waltham, Massachusetts) and 10mM HEPES (UCSF Media Core Facility) in the presence of $OVA_{257-264}$ peptide (0.1nM) (Invivogen, San Diego, California) and IL-2 (100U/ml) (Teceleukin) kindly provided by NCI Frederick. After 3 days in culture, activated cells were washed 3 times with RPMI 1640 and recultured in T25 culture flasks at $1*10^5$ cells/mL in the presence of either IL-7, IL-15 Biolegend, San Diego, California) or IL-2 (Teceleukin) kindly provided by NCI Frederick. (all cytokines 10ng/ml) After 2 additional days in culture, cells were passaged and recultured under the same conditions without peptide for an additional two days for total of 7 days in culture. Viability was confirmed by trypan blue exclusion (Thermo Fisher, Waltham, Massachusetts) or mass cytometry as described below.

Cell Preparation

All tissue preparations were performed simultaneously from each individual mouse, as previously reported (Spitzer et al. 2017). After euthanasia by CO_2 inhalation, spleens were collected and homogenized in PBS + 5mM EDTA at 4°C. All tissues were washed with PBS/EDTA and re-suspended 1:1 with PBS/EDTA and 100mM Cisplatin (Enzo Life Sciences, Farmingdale, NY) for 60s before quenching 1:1 with PBS/EDTA + 0.5% BSA to determine viability as previously described (Spitzer et al., 2015). Cells were centrifuged at 500 g for 5 min at 4°C and re-suspended in PBS/EDTA/BSA at a density between 1-10*10^6 cells/ml. Care was taken to maintain all samples at 4°C during all phases of tissue harvest and preparation except viability staining and fixation. Suspensions were fixed for 10 min at RT using 1.6% PFA (Fisher Scientific, Hampton, New Hampshire) and frozen at -80°C.

Mass-Tag Cellular Barcoding

Mass-tag cellular barcoding was performed as previously described (Zunder et al., 2015). Briefly, 1*10^6 cells from each animal were barcoded with distinct combinations of stable Pd isotopes in 0.02% saponin in PBS. Samples from any given tissue from each mouse per experiment group were barcoded together. Cells were washed once with cell staining media (PBS with 0.5% BSA and 0.02% NaN3), and once with 1X PBS, and pooled into a single FACS tube (BD Biosciences, San Jose, California). After data collection, each condition was deconvoluted using a single-cell debarcoding algorithm (Zunder et al., 2015).

Mass Cytometry Staining and Measurement

Cells were resuspended in cell staining media (PBS with 0.5% BSA and 0.02% NaN3), and antibodies against CD16/32 (BioLegend, San Diego, California) were added at 20 mg/ml for 5 min at RT on a shaker to block Fc receptors. Surface marker antibodies were then added, yielding 500 uL final reaction volumes and stained for 30 min at RT on a shaker. Following staining, cells were washed 2 times with cell staining media, then permeabilized with methanol for at 10 min at 4°C. Cells were then washed twice in cell staining media to remove remaining methanol, and stained with intracellular antibodies in 500 uL for 1 hour at RT on a shaker. Cells were washed twice in cell staining media and then stained with 1mL of 1:4000 191/193Ir DNA intercalator (Fluidigm, South San Francisco, CA) diluted in PBS with 4% PFA overnight. Cells were then washed once with cell staining media, once with 1X PBS and once with Cell Acquisition Solution (Fluidigm, South San Francisco, CA). Care was taken to assure buffers preceding analysis were not contaminated with metals in the mass range above 100 Da. Mass cytometry samples were diluted in Cell Acquisition Solution containing bead standards (see below) to approximately 10^6 cells per mL and then analyzed on a Helios mass cytometer (Fluidigm, South San Francisco, CA) equilibrated with Cell Acquisition Solution. We analyzed 1-5*10^5 cells per animal per time point, consistent with generally accepted practices in the field. For adoptive transfer experiments, 1-4*10^6 cells per animal were analyzed.

Mass Cytometry Bead Standard Data Normalization

Data normalization was performed as previously described (Spitzer et al., 2017). Briefly, just before analysis, the stained and intercalated cell pellet was resuspended in freshly prepared Cell Acquisition Solution containing the bead standard at a concentration ranging between 1 and 2*10^4 beads/ml. The mixture of beads and cells were filtered through a filter cap FACS tubes (BD Biosciences) before analysis. All mass cytometry files were normalized together using the mass cytometry data normalization algorithm (Finck et al., 2013), which uses the intensity values of a sliding window of these bead standards to correct for instrument fluctuations over time and between samples.

Adoptive T Cell Transfer

For adoptive transfer of transitional cells and SLECs, T cells were sorted by FACS from splenocytes harvested from WT CD45.2 C47Bl/6 mice or CD45.1 BoyJ mice 5 days post-infection. Then, viable sorted cells were counted by hemocytometer and Trypan blue staining, resuspended in sterile PBS and transferred into infection-matched congenic mice intravenously via the retroorbital vein.

For adoptive transfer of naïve pathogen specific T cells to validate the antigen specificity of transitional cells, CD8 T cells were immunomagnetically enriched from the spleens of CD45.1 OT1 TCR transgenic mice with EasySep Streptavidin Negative Selection using the following biotinylated antibodies: MHCII (AF6-120.1), CD11c (N418), Gr1 (RB6-8C5), B220 (RA3-6B2), CD4 (GK1.5), Ter119 (TER-119). Viable cells were quantified by counting on a hemocytometer with Trypan blue staining. Cells were then resuspended in sterile PBS and transferred into naïve WT CD45.2 mice intravenously via the retroorbital vein.

Flow Cytometry and Cell Sorting

Cells were stained for viability with Zombie-NIR dye. Cell surface staining was performed in cell staining media (PBS with 0.5% BSA and 0.02% NaN3) for 30 minutes at room temperature. The following anti-mouse antibodies were used: TCRβ – APC (H57-597), CD8 – PE (53-5.8), CD62L - BV421 (MEL-14), KLRG1 – BV510 (2F1/KLRG1), CD44 – PE-Cy7 (IM7), CD25 – FITC (3C7), CD19 – APC-Cy7 (1D3/CD19), F480 APC-Cy7 (BM8). Stained cells were analyzed with an LSR II flow cytometer (BD Biosciences). MitoTracker Deep Red (Thermo Fisher, Waltham, Massachusetts) staining was performed per manufacturer's instructions and as previously (Scharping et al, 2016).

For sorting experiments, cells were prepared as described for flow cytometry and then sorted into FBS containing media (RPMI 1640, 20% FBS, 1% HEPES, 100 mg/mL penicillin/streptomycin) on a FACSAria III (BD Biosciences).

Seahorse Assays

Seahorse Assays were carried out utilizing Agilent Mitochondrial Stress Test kit as previously (van der Windt et al, 2012) and per the manufacturer's instructions. Oxygen consumption rates (OCR) and extracellular acidification rates (ECAR) were measured in XF media (non-buffered RPMI 1640 containing 10 mM glucose, 2mM L-glutamine, and 1 mM sodium pyruvate) under basal conditions and in response to 1 μM oligomycin, 1 μM fluoro-carbonyl cyanide phenylhydrazone (FCCP) and 100 nM rotenone + 1 μM antimycin A (all from Agilent, Santa Clara, California) using a 96 well XF Extracellular Flux Analyzer (EFA) (Agilent, Santa Clara, California).

QUANTIFICATION AND STATISTICAL ANALYSIS

Statistical Analysis

All significance analysis of Seahorse data and cellular frequency was performed by paired two-sided student's t-test with error bars representing SEM in Prism v8. (GraphPad, San Diego, California).

Unsupervised Clustering Analysis

Cell clusters were identified using the Phenograph algorithm as implemented in the 'cytofkit' package in R. Standard settings were utilized (with k = 30).

Single-cell Scaffold Map Generation

Single-cell Scaffold maps were generated using the previously described open source Statistical Scaffold R package available at github.com/SpitzerLab/statisticalScaffold. To generate Scaffold Maps plotting each single cell instead of clusters, we modified the code to generate .Rdata and .txt files from FCS files that contain ASINH (cofactor 5) transformed expression values for all recorded parameters as well as a cell ID number. These modified .Rdata and .txt files were then utilized for the generation of Scaffold Maps by combining single cells and manually gated landmark reference nodes (using median marker expression values) in a force directed graph. The highest-scoring edge from each single cell connecting to the nearest landmark reference node was used to categorize single cells.

Data Visualization

Unsupervised force-directed graphs were generated as previously reported (Spitzer et al., 2015) with the following modifications. Single cells were downsampled to n = 500 cells from each condition. All cells were combined in a single graph with edge weights defined as the cosine similarity between the vectors of marker values of each cell. All the pairwise distances were calculated and for each node only the 10 edges of highest weight were retained. The graph was then laid out using the ForceAtlas2 algorithm in Gephi.

DATA AVAILABILITY

Mass cytometry data will be made publicly available as a report on Cytobank (www.cytobank.org) with linked flow cytometry standard (.fcs) files upon acceptance of the manuscript.

Figure 1

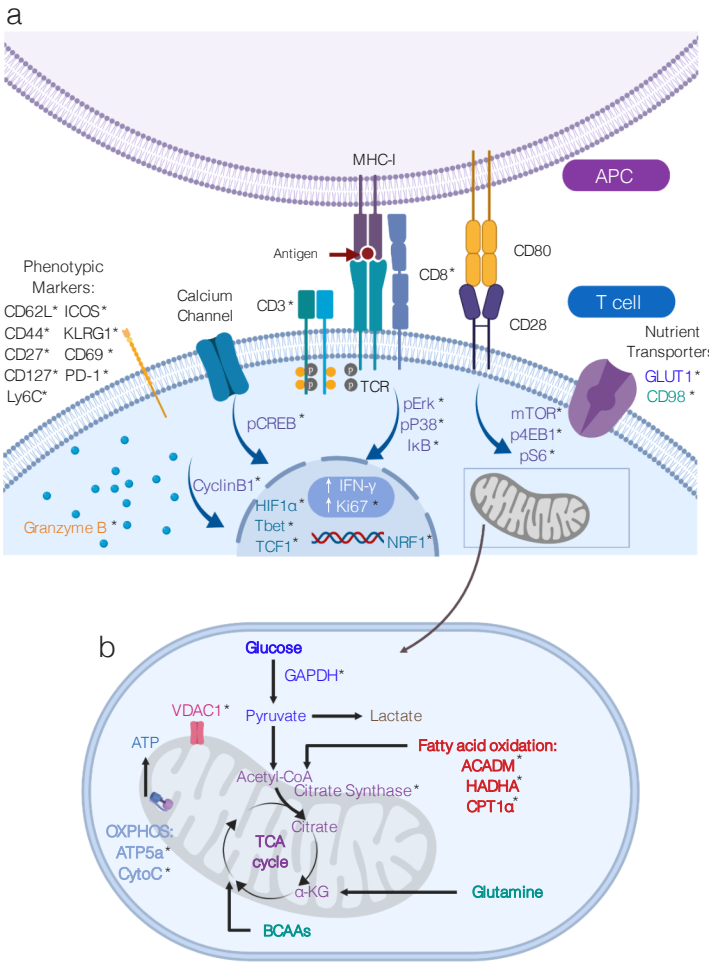
a
MHC-I
APC
Antigen
CD8*
CD80
CD28
T cell
Phenotypic Markers:
CD62L* ICOS*
CD44* KLRG1*
CD27* CD69 *
CD127* PD-1*
Ly6C*
Calcium Channel
CD3*
TCR
Nutrient Transporters:
GLUT1*
CD98 *
pCREB *
pErk *
pP38*
IkB *
mTOR*
p4EB1*
pS6*
CyclinB1*
↑ IFN-γ
↑ Ki67 *
HIF1α *
Tbet *
TCF1*
NRF1*
Granzyme B *
b
Glucose
GAPDH*
VDAC1*
Pyruvate
Lactate
ATP
Fatty acid oxidation:
ACADM*
HADHA*
CPT1α*
Acetyl-CoA
Citrate Synthase*
Citrate
OXPHOS:
ATP5a*
CytoC *
TCA cycle
α-KG
Glutamine
BCAAs

Figure 2

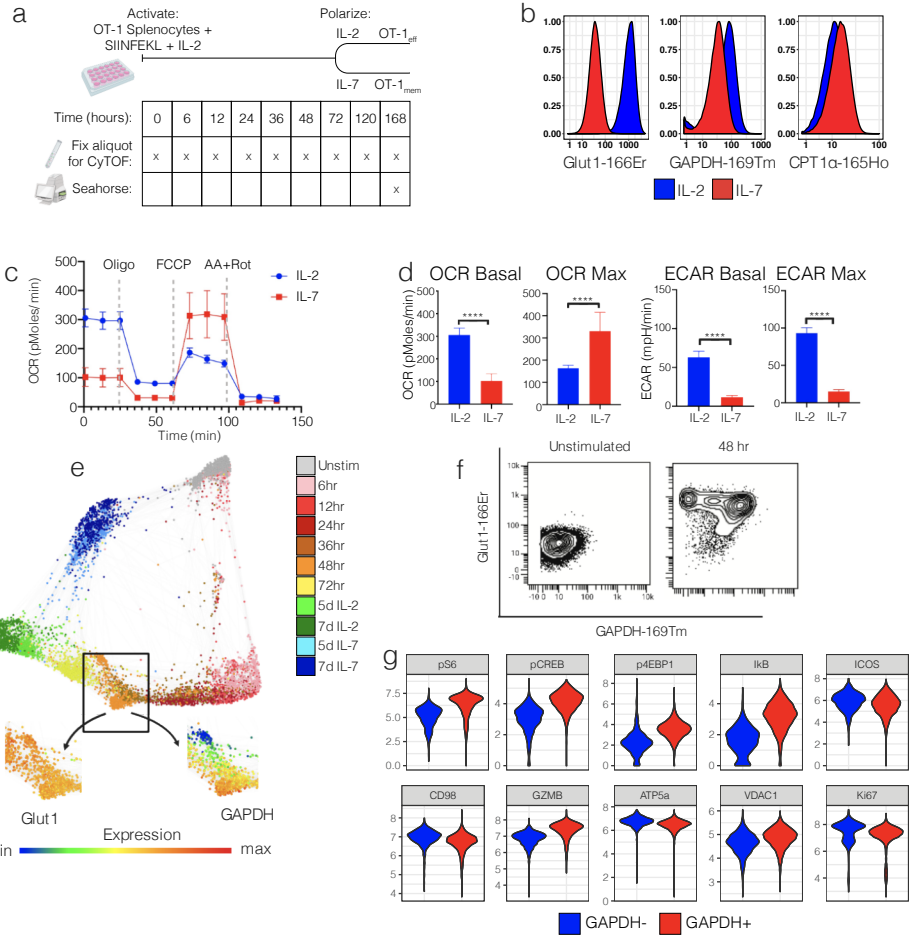
a
Activate:
OT-1 Splenocytes +
SIINFEKL + IL-2
Polarize:
IL-2
OT-1eff
IL-7
OT-1mem
Time (hours): 0 6 12 24 36 48 72 120 168
Fix aliquot for CyTOF: x x x x x x x x x
Seahorse: x
b
Glut1-166Er
GAPDH-169Tm
CPT1α-165Ho
IL-2
IL-7
c
Oligo
FCCP
AA+Rot
IL-2
IL-7
OCR (pMoles/min)
Time (min)
d
OCR Basal
OCR Max
ECAR Basal
ECAR Max
OCR (pMoles/min)
ECAR (mpH/min)
****
IL-2
IL-7
e
Unstim
6hr
12hr
24hr
36hr
48hr
72hr
5d IL-2
7d IL-2
5d IL-7
7d IL-7
Glut1
GAPDH
Expression
min
max
f
Unstimulated
48 hr
Glut1-166Er
GAPDH-169Tm
g
pS6
pCREB
p4EBP1
IkB
ICOS
CD98
GZMB
ATP5a
VDAC1
Ki67
GAPDH-
GAPDH+

Figure 3

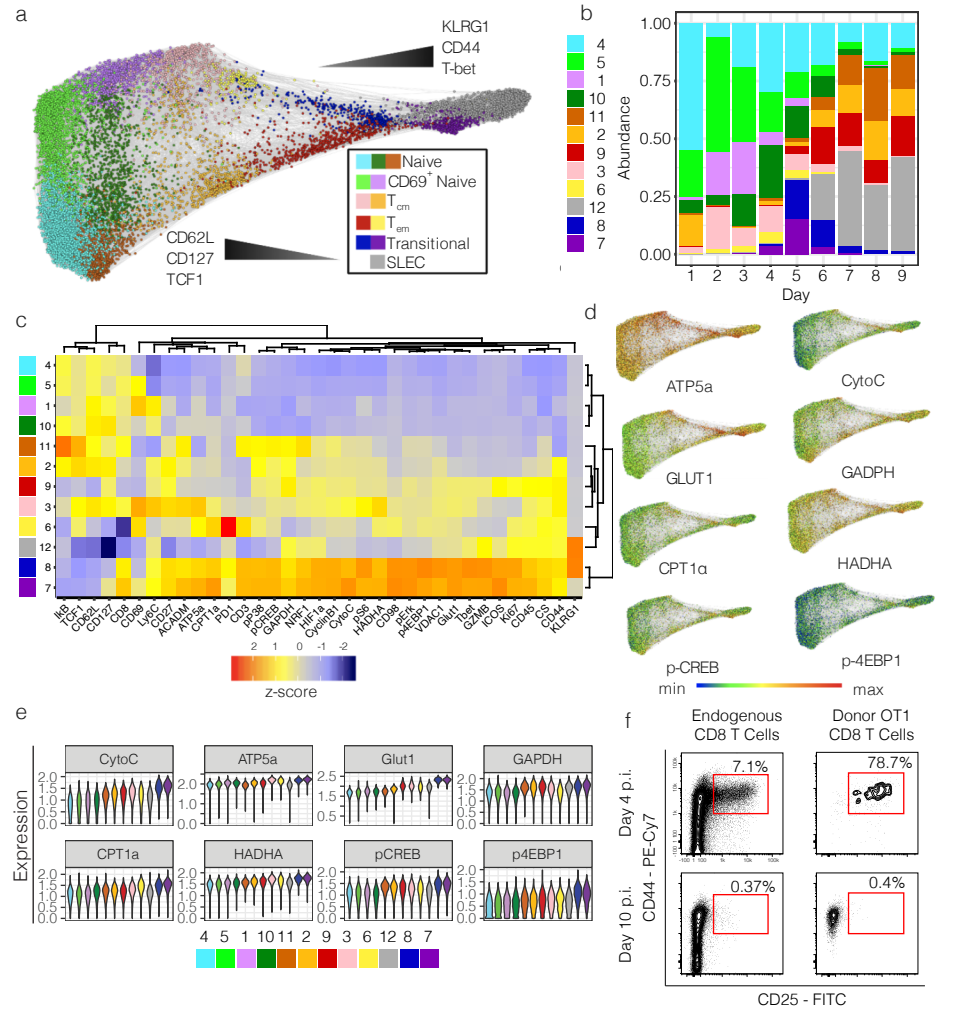
a
KLRG1
CD44
T-bet
CD62L
CD127
TCF1
Naive
CD69+ Naive
Tcm
Tem
Transitional
SLEC
b
Abundance
Day
c
z-score
d
ATP5a
CytoC
GLUT1
GADPH
CPT1α
HADHA
p-CREB
p-4EBP1
min
max
e
Expression
CytoC
ATP5a
Glut1
GAPDH
CPT1a
HADHA
pCREB
p4EBP1
f
Endogenous CD8 T Cells
Donor OT1 CD8 T Cells
Day 4 p.i.
Day 10 p.i.
7.1%
78.7%
0.37%
0.4%
CD44 - PE-Cy7
CD25 - FITC

Figure 4

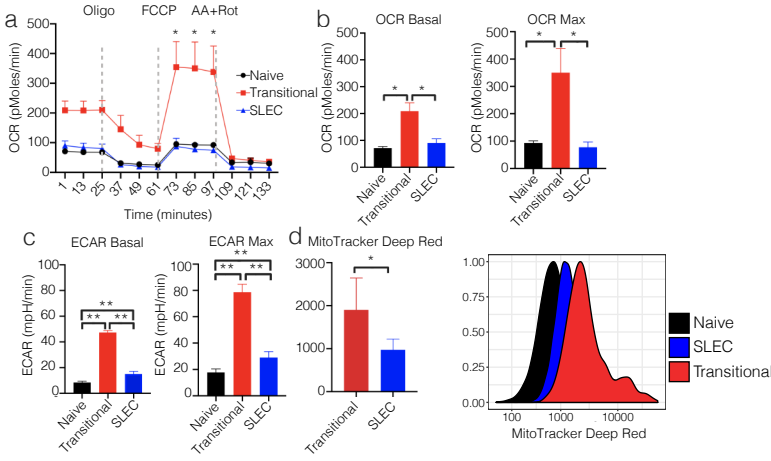
a
Oligo
FCCP
AA+Rot
OCR (pMoles/min)
Time (minutes)
Naive
Transitional
SLEC
b
OCR Basal
OCR Max
OCR (pMoles/min)
Naive
Transitional
SLEC
c
ECAR Basal
ECAR Max
ECAR (mpH/min)
Naive
Transitional
SLEC
d
MitoTracker Deep Red
Transitional
SLEC
MitoTracker Deep Red
Naive
SLEC
Transitional

Figure 5

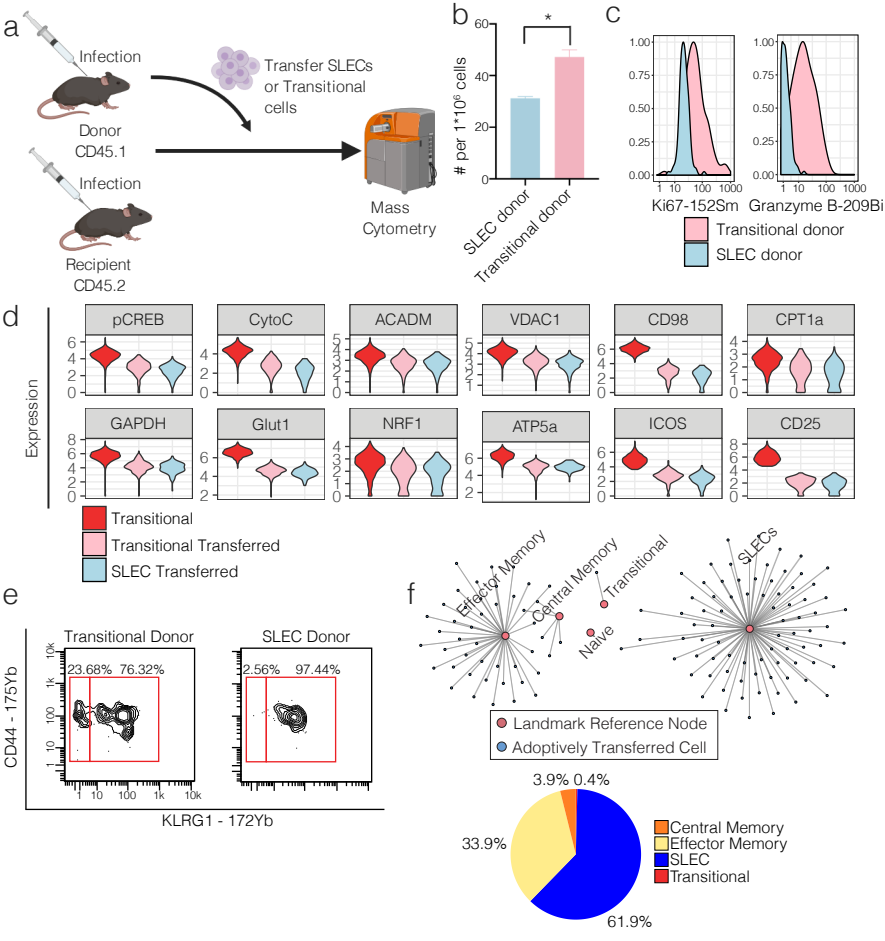
a
Infection
Donor
CD45.1
Infection
Recipient
CD45.2
Transfer SLECs
or Transitional
cells
Mass
Cytometry
b
per 1*10^6 cells
SLEC donor
Transitional donor
c
Ki67-152Sm
Granzyme B-209Bi
Transitional donor
SLEC donor
d
Expression
pCREB
CytoC
ACADM
VDAC1
CD98
CPT1a
GAPDH
Glut1
NRF1
ATP5a
ICOS
CD25
Transitional
Transitional Transferred
SLEC Transferred
e
Transitional Donor
SLEC Donor
23.68% 76.32%
2.56% 97.44%
CD44 - 175Yb
KLRG1 - 172Yb
f
Effector Memory
Central Memory
Transitional
Naïve
SLECs
Landmark Reference Node
Adoptively Transferred Cell
3.9% 0.4%
33.9%
61.9%
Central Memory
Effector Memory
SLEC
Transitional

Figure S1

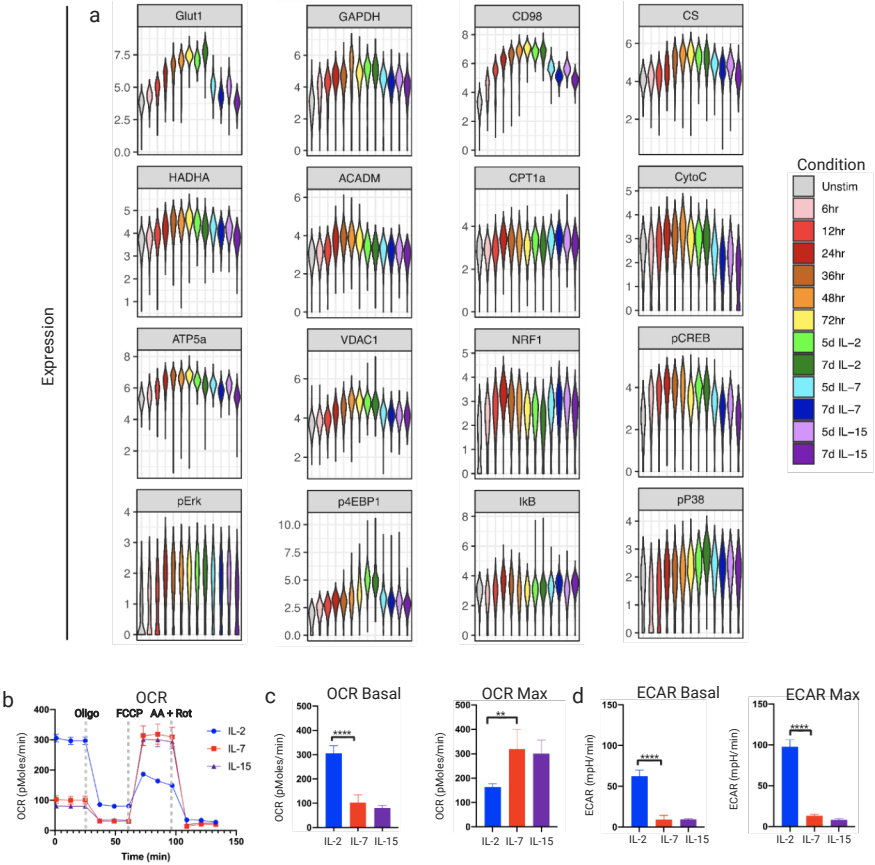
a
Expression
Glut1
GAPDH
CD98
CS
HADHA
ACADM
CPT1a
CytoC
ATP5a
VDAC1
NRF1
pCREB
pErk
p4EBP1
IkB
pP38
Condition
Unstim
6hr
12hr
24hr
36hr
48hr
72hr
5d IL-2
7d IL-2
5d IL-7
7d IL-7
5d IL-15
7d IL-15
b
OCR
Oligo
FCCP
AA + Rot
IL-2
IL-7
IL-15
OCR (pMoles/min)
Time (min)
c
OCR Basal
OCR Max
OCR (pMoles/min)
IL-2
IL-7
IL-15
d
ECAR Basal
ECAR Max
ECAR (mpH/min)

Figure S2

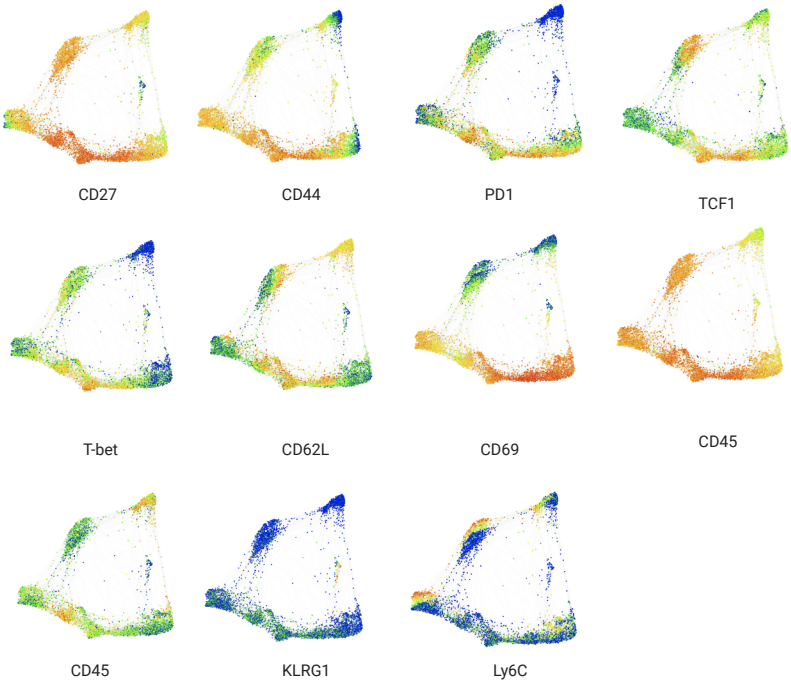

Figure S3

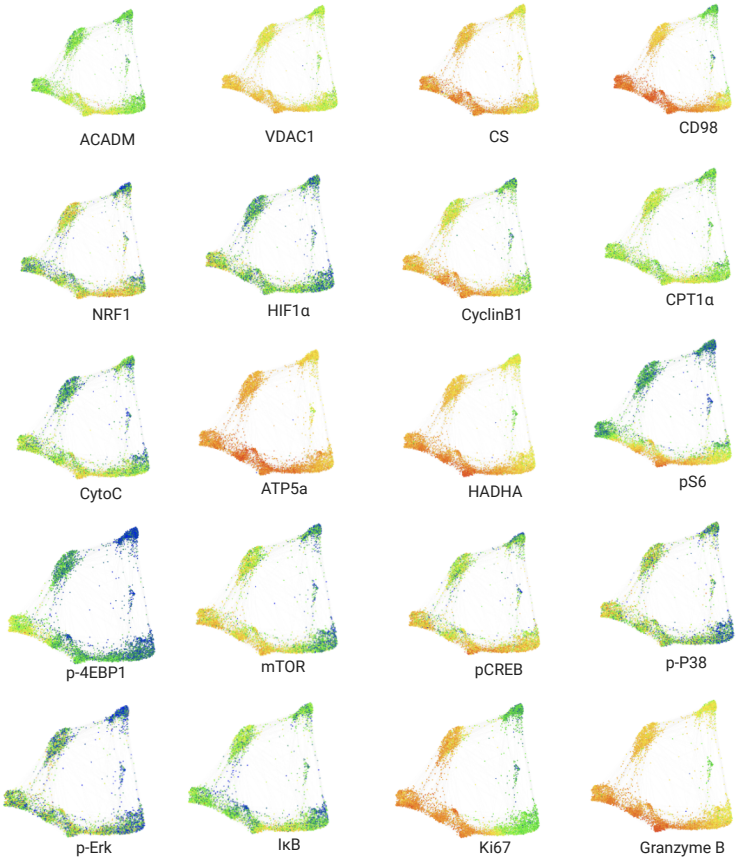
ACADM
VDAC1
CS
CD98
NRF1
HIF1α
CyclinB1
CPT1α
CytoC
ATP5a
HADHA
pS6
p-4EBP1
mTOR
pCREB
p-P38
p-Erk
IκB
Ki67
Granzyme B

Figure S4

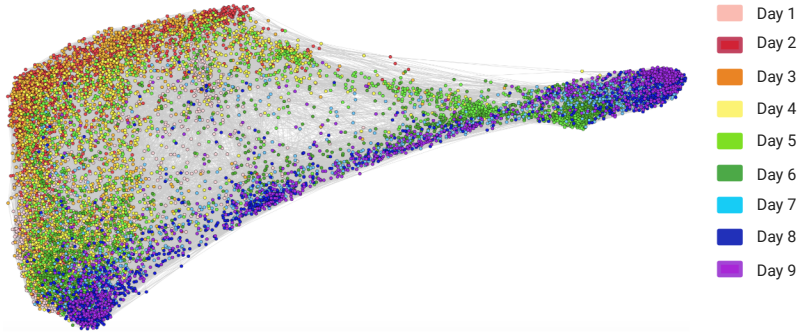

Figure S5

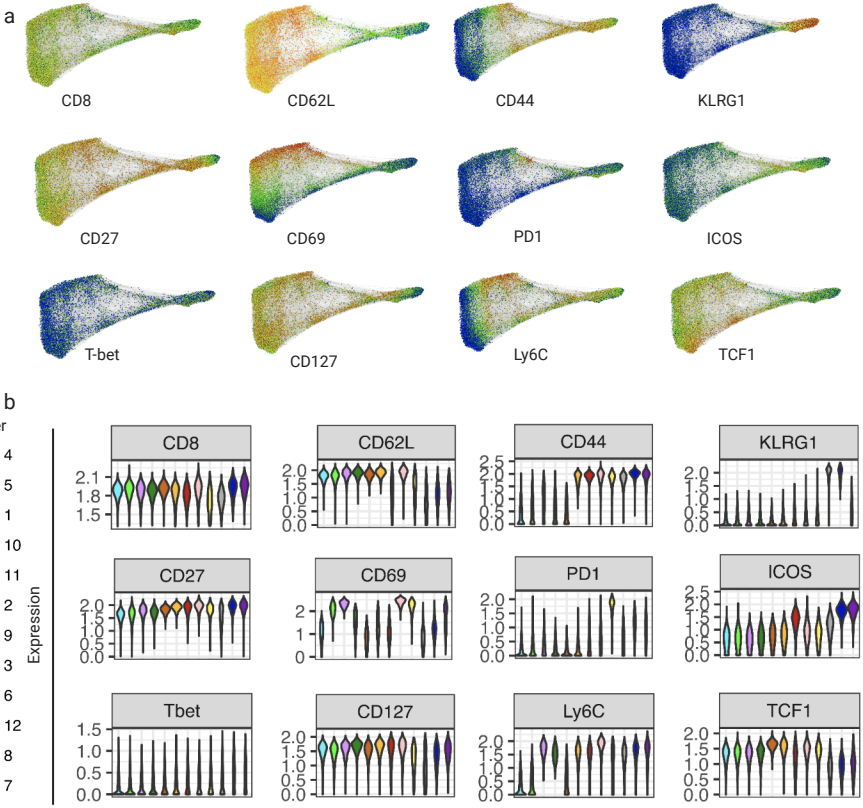
a
CD8
CD62L
CD44
KLRG1
CD27
CD69
PD1
ICOS
T-bet
CD127
Ly6C
TCF1
b
Cluster
4
5
1
10
11
2
9
3
6
12
8
7
Expression
CD8
CD62L
CD44
KLRG1
CD27
CD69
PD1
ICOS
Tbet
CD127
Ly6C
TCF1

Figure S6

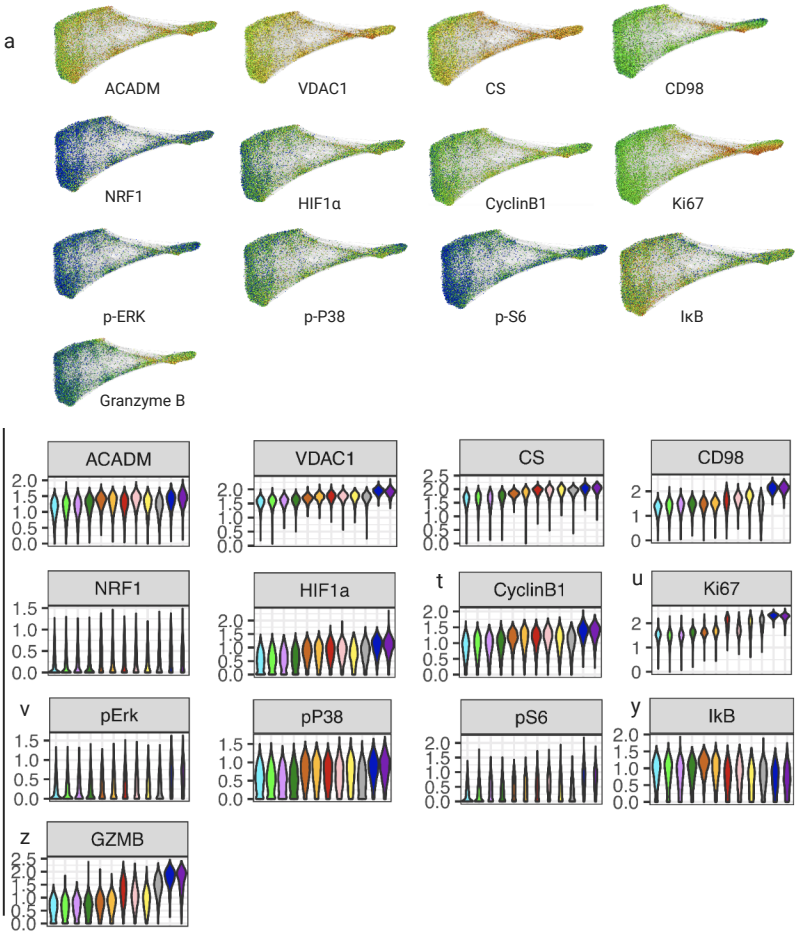
a
ACADM
VDAC1
CS
CD98
NRF1
HIF1α
CyclinB1
Ki67
p-ERK
p-P38
p-S6
IκB
Granzyme B
b
Cluster
4
5
1
10
11
2
9
3
6
12
8
7
Expression
ACADM
VDAC1
CS
CD98
NRF1
HIF1a
t
CyclinB1
u
Ki67
v
pErk
pP38
pS6
y
IkB
z
GZMB

Figure S7

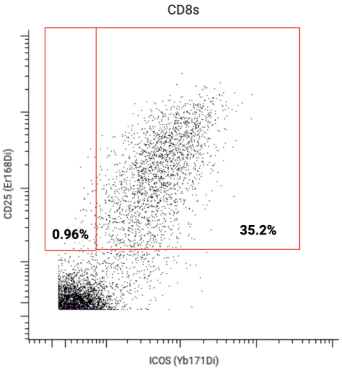
CD8s
CD25 (Er168Di)
ICOS (Yb171Di)
0.96%
35.2%

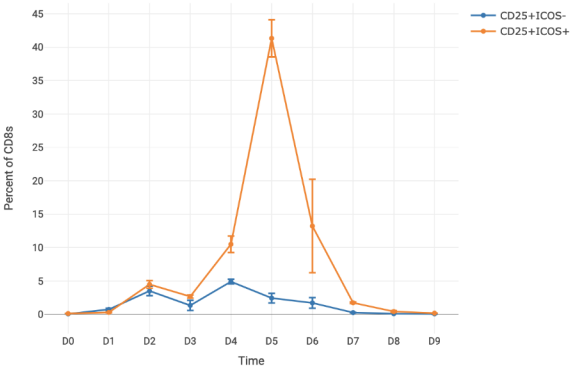
CD25+ICOS-
CD25+ICOS+
Percent of CD8s
Time
0
5
10
15
20
25
30
35
40
45
D0
D1
D2
D3
D4
D5
D6
D7
D8
D9

Figure S8

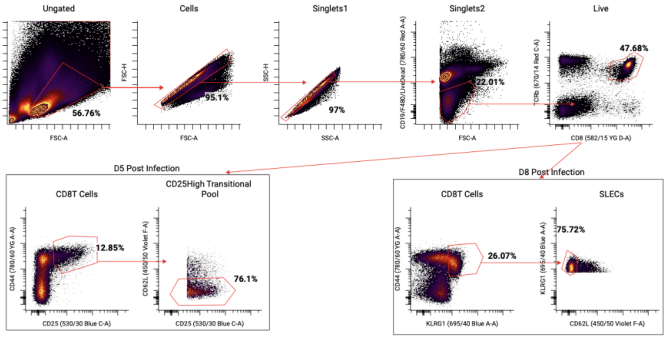

Ungated
Cells
Singlets1
Singlets2
Live
56.76%
95.1%
97%
22.01%
47.68%
FSC-A
FSC-H
SSC-A
SSC-H
CD19/F480/LiveDead (780/60 Red A-A)
CD8 (582/15 YG D-A)
D5 Post Infection
CD8T Cells
CD25High Transitional Pool
12.85%
76.1%
CD44 (780/60 YG A-A)
CD25 (530/30 Blue C-A)
CD62L (450/50 Violet F-A)
D8 Post Infection
CD8T Cells
SLECs
26.07%
75.72%
KLRG1 (695/40 Blue A-A)
CD62L (450/50 Violet F-A)

Table S1

Marker	Vendor	Catalog No.	Clone	Channel	[Optimal](μg/mL)
Ter119	BioLegend	116202	TER-119	89	6
CD45.2	BioLegend	109802	104	113	3
CD45.1	BioLegend	110702	A20	115	3
CD4	BioLegend	100506	RMA4-5	139	6
CD8	BioLegend	100702	53-6.7	140	6
CD38	Biolegend	102702	90	141	6
HADHA	Abcam	ab231169	EPR17940	142	6
Ly6C	BioLegend	128002	HK1.4	143	0.375
pS6	CST	Custom	2F9	144	3
pCREB	CST	9198BF	87G3	145	1.5
NRF1	Abcam	ab221792	EPR5554(N)	146	3
CD98	BioLegend	128202	RL388	147	3
Cyclin B1	BD	Custom	GNS1	148	6
CytoC	BioLegend	612302	6H2.B4	149	0.75
T-bet	BioLegend	644802	4B10	150	6
pErk	CST	Custom	D13	151	6
Ki67	Thermo/eBioscience	11-5698-82	SolA15	152	6
CS	Abcam	ab233838	EPR8067	153	0.75
MTOR	CST	Custom	7C10	154	6
HIF1a	Thermo/Invitrogen	700505	16H4L13	155	6
CD62L	R&D	MAB5761	95218	156	1.5
TCRgd	BioLegend	118101	GL3	157	1.5
ACADM	Abcam	ab110296	3B7BH7	158	6
CD127	BioLegend	135002	A7R34	159	6
ATP5a	Abcam	ab110273	7H10BD4F9	160	6
VDAC1	Abcam	ab14734	20B12AF2	161	6
p4EBP1	CST	2855BF	236B4	162	6
ikBα	CST	4614BF	L35A5	163	3
TCF1/TCF7	CST	2203BF	C63D9	164	6
CPT1a	Abcam	ab128568	8F6AE9	165	6
Glut1	Abcam	ab196357	EPR3915	166	0.75
Foxp3	Thermo	Custom	NRRF-30	167	3
p-p38	BD Pharmingen	Custom	36/p38	168	1.5
CD25	BioLegend	102014	PC61	168	3
GAPDH	Thermo	AM4300	6C5	169	1.5
CD3	BioLegend	100202	17A2	170	3
ICOS	BioLegend	313502	C398.4A	171	3
KLRG1	BioLegend	368602	2F1	172	0.75
PD1	BioLegend	135202	29F.1A12	173	0.75
CD69	R&D	AF2386	polyclonal	174	6
CD44	BioLegend	103002	IM7	175	0.375
CD27	BioLegend	124202	LG.3A10	176	1.5
Granzyme B	BioLegend	372202	QA16A02	209	0.75